Research Article | Vol. 33, No. 11 / 2 Jun 2025 / Optics Express 24130

Optics EXPRESS

Sources of nonlinearity and mitigation of phase noise in MUTC photodetectors at comb-line frequencies

ISHRAQ MD ANJUM,[1,*] ERGUN SIMSEK,[1] SEYED EHSAN JAMALI MAHABADI,[1] THOMAS F. CARRUTHERS,[1] CURTIS R. MENYUK,[1] JOE C. CAMPBELL,[2] DAVID A. TULCHINSKY,[3] AND KEITH J. WILLIAMS[3]

[1]*Department of Computer Science and Electrical Engineering, University of Maryland, Baltimore County, Baltimore, MD 21250, USA*
[2]*Department of Electrical and Computer Engineering, University of Virginia, Charlottesville, VA 22904, USA*
[3]*Naval Research Laboratory, Washington, DC 20375, USA*
[*]*ianjum1@umbc.edu*

Abstract: We calculate the phase noise for the first 100 comb line frequencies of two modified uni-traveling-carrier (MUTC) photodetectors. The frequency comb is generated by one-picosecond pulses with a 2-GHz repetition frequency. We observe a non-monotonic increase in the phase noise and investigate its origins. Our model identifies the interplay among the space charge effect, the heterostructure design, and the nonlinear relationship between the electric field and the electron drift current that leads to a complex variation of the phase noise as a function of the comb line frequency. Based on the findings, we present ways to reduce the phase noise of the photodetectors. While the optimal design depends on the desired frequency range of operation, we find a design that can reduce the phase noise over a wide range of comb-line frequencies.

1. Introduction

Modern epitaxial technology enables high-precision control of the doping and composition profile of compound semiconductor devices, while advances in computational power and numerical techniques aid us to design, optimize and understand the operation of these devices. Simulations based on the drift-diffusion equations constitute an attractive technique for simulating photodetectors [1,2]. The drift-diffusion model is a useful compromise between Monte Carlo techniques and purely empirical models. Monte Carlo techniques take into account the full band structure, but are too slow computationally to model modern-day devices with complex structures [3]. Purely empirical models have little predictive capability.

A uni-traveling-carrier photodiode (UTC) [4] inhibits the motion of photogenerated holes and only uses electrons as active carriers in the device. Eliminating holes as active carriers increases the bandwidth of the device since electrons are more mobile than holes; however, space charge effects continue to limit the bandwidth. A modified UTC (MUTC) photodetector has been designed by Z. Li *et al*. [5] in which the space charge effect is reduced by adding a cliff layer between the collection and the absorption layers.

In RF-photonics, time and frequency metrology, and photonic low-phase-noise generation, MUTC photodetectors are often used due to their large bandwidth and large dynamic range. However, phase noise generated in the photodetectors can limit the system performance in these applications [10]. In particular, phase noise limits the transfer of the low noise of an optical frequency comb to the microwave domain [11]. In this work, we use the drift-diffusion equations

#562682 https://doi.org/10.1364/OE.562682
Journal © 2025 Received 19 Mar 2025; revised 15 May 2025; accepted 20 May 2025; published 30 May 2025

to calculate, analyze, and find ways to reduce the phase noise at comb-line frequencies in MUTC photodetectors.

Due to the important role that photodetectors—and in particular MUTC photodetectors—play in limiting the performance of frequency combs, there has been a steady interest in finding efficient ways to calculate the phase noise that they produce and to optimize the device structures to minimize the noise at the frequencies of interest [6,7]. Quinlan *et al*. [7] predicted that phase noise in ultrashort optical pulse trains decreases and approaches zero as pulse duration shortens. Experiments later showed that this reduction plateaus when the optical pulse becomes much shorter than the resulting electrical pulse from the photodetector [8,9]. Sun *et al*. [3] confirmed these observations using Monte Carlo simulations that included collisional diffusion of electrons, but this approach is computationally time-consuming. Jamali Mahabadi *et al*. [9] showed that it is possible to calculate phase noise by first calculating the impulse response of a photodetector from the drift-diffusion equations and then taking advantage of the Poisson distribution of electrons in any time slot to calculate the phase noise using simple integrals over the impulse response. This approach greatly reduces the computation time and simplifies both the calculation and the physical interpretation of the results.

Jamali Mahabadi *et al*. [9] calculated the phase noise at the 10-GHz comb-line frequency in MUTC photodetector (MUTC-4) that was designed by Li *et al*. [5] and that we show in Fig. 1(a). Here we extend the work of Jamali Mahabadi *et al*. by calculating the phase noise at the first 100 comb-line frequencies [12] in the MUTC-4 photodetector and in a more-recently designed MUTC photodetector (MUTC-9) that was fabricated by Zang *et al*. [13]. We focus on these two MUTC photodetectors for study since the MUTC-4 was previously investigated in the context of phase noise [9], while the MUTC-9 was subsequently adopted for use at NIST [6]. We focus here on the shot noise due to the random variations in the electron arrival time at the output of the device. While amplitude-to-phase noise conversion can also be an important source of noise in some applications [14,15], its effect can be greatly mitigated in comb applications by careful choice of the bias point [16] or through use of a charge-compensated MUTC [13]. We find that the phase noise due to shot noise increases non-monotonically as a function of comb-line frequency and comb-line number in contrast to the van der Linde prediction [17]. We investigate the reason for the non-monotonic increase of the phase noise and find new device configurations that reduce the phase noise. The work extends prior work [18] by giving a detailed description of the computational model, phase noise calculation, and the phase noise physics and by including new results in which we optimize the photodetector structure to reduce the phase noise.

2. Computational model

We use the one-dimensional (1-D) computational model based on the drift-diffusion equations that was developed by Hu *et al*. [19] and improved upon by Simsek *et al*. [20,21]. We take into account impact ionization [22], carrier recombination, thermionic emission [23], the Franz-Keldysh effect [24,25], and quantum tunneling [23]. We use a velocity model that depends on the electric field, doping density, and temperature. We follow the procedure described by Jamali Mahabadi *et al*. [9] to calculate the phase noise. The equation for calculating the phase noise from the impulse response is:

$$\left\langle \Phi_n^2 \right\rangle = \frac{1}{N_{\mathrm{tot}}} \frac{\int_0^{T_R} h_e(t) \sin^2 \left[2\pi n(t-t_c)/T_R\right] \mathrm{d}t}{\left\{\int_0^{T_R} h_e(t) \cos \left[2\pi n(t-t_c)/T_R\right] \mathrm{d}t\right\}^2}, \tag{1}$$

where Φ_n^2 is the mean square phase fluctuation at comb-line number n, N_{tot} is the total number of electrons in the one pulse of the photocurrent, T_R is the repetition period, $h_e(t)$ is the electronic

Optics EXPRESS

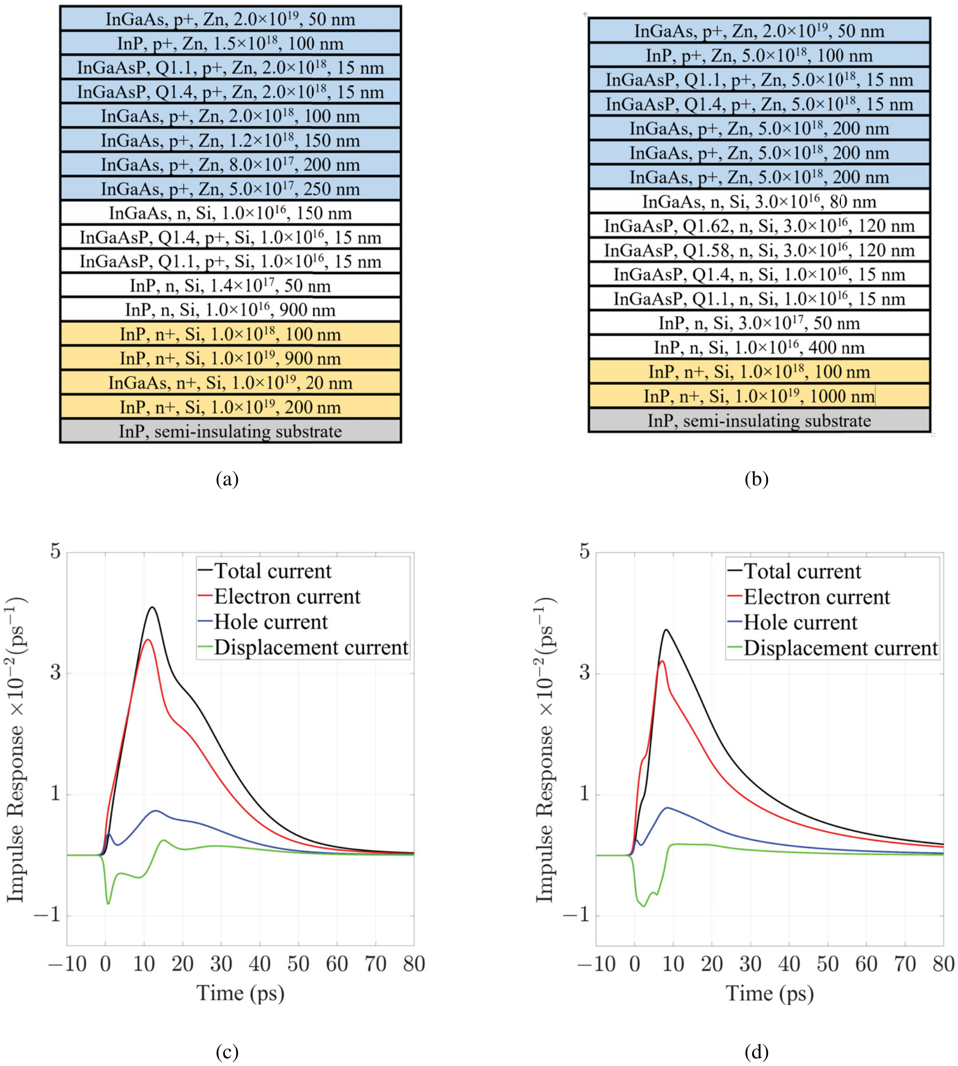

Fig. 1. Structures of the (a) MUTC-4 and (b) MUTC-9 photodetectors. Blue indicates the *p*-region, yellow indicates the *n*-region, white indicates the *i*-region, and grey indicates the substrate. Normalized impulse response of the (c) MUTC-4 and (d) MUTC-9 photodetectors.

impulse response, and $t_c(n)$ is the central time of the output current defined by the relation:

$$\int_0^{T_R} \langle i_n(t) \rangle \sin\left[\frac{2\pi n}{T_R}(t - t_c)\right] \mathrm{d}t = 0, \tag{2}$$

where $\langle i_n(t) \rangle$ is the average current in the n-th frequency comb line, which in our noise-free simulations simply equals the comb line current. The electronic impulse response is given by

$$h_e(t) = \frac{\Delta I_{\text{out}}(t)}{\int_0^{\infty} \Delta I_{\text{out}}(t) dt}, \tag{3}$$

where $\Delta I_{\text{out}}(t)$ is the change in the output current due to an instantaneous light pulse.

Optics EXPRESS

3. Phase noise results

In Fig. 1(a) we show the MUTC-4 structure and in Fig. 1(b) we show the MUTC-9 structure that we study. In this work, the output current I_{out} is set to 10 mA, the bias voltage V_{bias} is set to 15 V, the external load impedance R_{load} is set to 50 Ω, and the diameter of the MUTC photodetectors is set to 30 μm. The input pulse duration is set to 1 ps and the repetition frequency is set to 2 GHz. We select the operating conditions based on the previous studies on phase noise in photodetectors for frequency comb applications [3,9] with adjustments to be more consistent with the parameters used at NIST [16]. The dependence of phase noise on operating conditions — bias voltage and output current — is illustrated in Fig. 7 of [9]. The 3-dB bandwidths of the MUTC-4 and MUTC-9 are about 17 GHz and 13 GHz respectively. The response time of the MUTC-4 is limited by a combination of RC and transit-time effects, while the response time of the MUTC-9 is primarily limited by RC effects. In order to calculate the impulse response we excite the photodetectors with a hyperbolic secant pulse. We plot the calculated impulse responses of the photodetectors in Figs. 1(c) and 1(d).

We plot the calculated phase noise and power spectra of MUTC-4 and MUTC-9 photodetectors in Figs. 2(a) and 2(b), assuming a repetition frequency of 2 GHz, as was used by [3]. In Fig. 2(c) and 2(d), we show an expanded view of the phase noise and power spectrum up to 20 GHz, which is the current range of operation for most frequency combs. The system performance will often be limited in practice by the electronic system in which the photodetector is embedded. For that reason, we chose to focus on understanding the internal physics of the device operation. In Figs. 2(a) and 2(b), we observe that phase noise generally increases as frequency increases. However, the increase is not monotonic, and is far more complex than the quadratic dependence predicted by van der Linde [17] due to the complicated nonlinear electron transport through the device. To better understand this complex behavior, we separately plot the numerator and denominator of Eq. (1) as functions of frequency in Figs. 2(e) and 2(f) respectively. The numerator and denominator correspond to the mean-square in-phase and quadrature components of each harmonic, respectively. We note that the mean-square quadrature component (numerator) is entirely due to current fluctuations. As the frequency increases, the numerator increases rapidly up to about 20 GHz and then becomes nearly flat. The limit when $n \to \infty$ is given by

$$\lim_{n\to\infty} \int_0^L h_e(t) \sin^2\left[\frac{2\pi n}{L}(t - t_c)\right] dt = \frac{1}{2}, \tag{4}$$

where we note using Eq. (3) that $\int_0^L h_e(t)\,dt = 1$. We repeat Eq. 1 here and define the numerator N_n and denominator D_n as follows:

$$\langle \Phi_n^2 \rangle = \frac{1}{N_{\text{tot}}} \frac{\int_0^{T_R} h_e(t) \sin^2\left[2\pi n(t - t_c)/T_R\right] \mathrm{d}t}{\left\{\int_0^{T_R} h_e(t) \cos\left[2\pi n(t - t_c)/T_R\right] \mathrm{d}t\right\}^2} = \frac{1}{N_{\text{tot}}} \frac{N_n}{D_n}. \tag{5}$$

For the 2-GHz repetition frequency that we are considering, we can simplify Eq. (1) for phase noise at frequencies above 20 GHz, which then becomes

$$\left\langle \Phi_n^2 \right\rangle \approx \frac{1}{2N_{\text{tot}} \left\{\int_0^{T_R} h_e(t) \cos\left[2\pi n(t - t_c)/T_R\right] \mathrm{d}t\right\}^2} = \frac{1}{2N_{\text{tot}}|H(f)|^2}. \tag{6}$$

In Fig. 2(f) we see that as frequency increases, the denominator D_n that corresponds to the mean-square in-phase component of the signal generally decreases as the frequency increases, although its behavior is non-monotonic, particularly for the MUTC-4. The complicated behavior of the phase noise spectrum is entirely due to the behavior of the denominator. Figure 2(b) shows

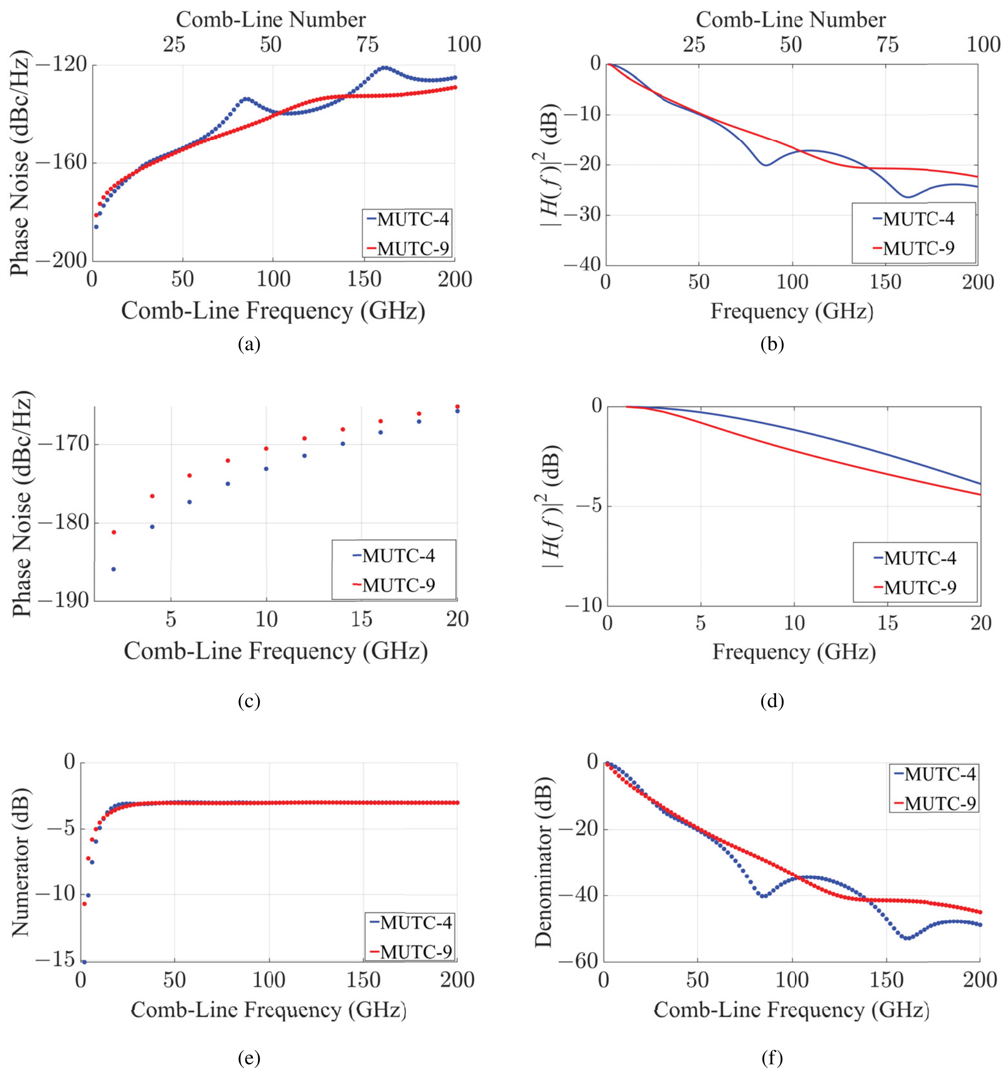

Fig. 2. (a) Phase noise (b) power spectrum vs. comb line frequency; expanded views of the (c) phase noise and (d) power spectrum below 20-GHz; (e) numerator N_n, and (f) denominator D_n of Eq. 5 in dB relative to 1 $A^2 \cdot s^2$.

that the power spectrum decreases non-monotically in a complicated fashion that mirrors the complexity in the phase noise. The complications are caused by the complex carrier transport inside the photodetector, which we will examine in the next section.

4. Impulse response carrier transport analysis

Upon illumination, electron-hole pairs are generated in the absorption region. The photogenerated electrons and holes drift and diffuse towards the contacts. In MUTC photodetectors, electrons are the majority carriers, and the electron drift current is much higher than the electron diffusion current in non-equilibrium under bias voltage. Hence, the electron drift current plays a greater role in determining the shape of the MUTC photodetector impulse response. While moving

Optics EXPRESS

across the photodetector, electrons transit through different layers, which have different electron drift velocity profiles as the electric field varies. When there is a change in the electron velocity profile of the majority electrons, we see a change in the slope of the impulse response. In the MUTC-9, we see the first change at 1 ps when the electrons pass through the four InGaAsP layers in the intrinsic region, as Fig. 1 indicates. In the MUTC-4, the slope change is more subtle since the thickness of the InGaAsP layers in the intrinsic region is 30 nm, compared to 270 nm in the MUTC-9.

We observe a fluctuation in the impulse response tail of the MUTC-4 at 21 ps that is absent in the MUTC-9 impulse response tail. As the photogenerated pulse of electrons is driven across the intrinsic region, a negative electric field is created in the last layer of the *p*-region as can be seen in Figs. 3(a) and 3(b) in which we show the electric field in the photodetectors after 1 ps of evolution. The entire field evolution may also be viewed in Visualization 1 for the MUTC-4 and Visualization 2 for the MUTC-9. These negative fields first appear in the MUTC-4 and in the MUTC-9 at 1 ps. This negative electric field causes negative electron and hole drift currents and traps a portion of the photogenerated electrons and holes as shown in Figs. 3(c) and 3(d). In the MUTC-4, the last InGaAs layer in the *p*-region has a lower doping density compared to the MUTC-9, so this layer in the MUTC-4 responds more strongly to the electric field. Hence, this layer has a higher and longer-lasting negative electric field in the MUTC-4, with a duration from −1 to 6.6 ps, compared to the MUTC-9, where it lasts from −1 to 5 ps, as can be seen in Visualization 1 and Visualization 2 respectively. In addition, the MUTC-4 has a lower steady-state electric field at the first intrinsic InGaAs layer. Due to the space charge effect, the electric field becomes increasingly negative, facilitating higher electron drift velocity. So, in the MUTC-4, after the negative electric field subsides, the trapped electrons entering the intrinsic region drift at a higher velocity compared to the MUTC-9. As a result, a batch of trapped electrons transiting through the intrinsic region forms and then travels as a secondary pulse in the MUTC-4 compared to the MUTC-9, where the second batch of electrons arrives at and passes through the intrinsic region gradually. The second electron drift current pulse in the MUTC-4 can be observed after the first pulse in the intrinsic region between 15 to 25 ps in Visualization 3 and the absence of a second electron drift current pulse in the MUTC-9 can be observed in Visualization 4. The transit of the trapped electrons in the form of a secondary pulse causes a fluctuation in the tail of the impulse response of the MUTC-4 at 21 ps. Although a higher electron drift velocity causes the fluctuation, it actually helps the electrons move through the intrinsic region faster, so that the the MUTC-4 impulse response has a shorter tail.

The electric field distributions of the MUTC-4 and MUTC-9 photodetectors in Figs. 3(a) and 3(b) exhibit a noticeable difference in the *p*-region. In the MUTC-4, there are electric fields at the *p*-region layer boundaries, as indicated inside the inset of Fig. 3(a), that are absent in the MUTC-9. The electric fields in the *p*-region layer boundaries help move the electrons out more quickly so that the tail of the MUTC-4 impulse response is shorter than that of the MUTC-9. We observe a large negative spike in both the electric field and electron drift velocity in the MUTC-4 that occurs at the heterojunction boundary at 3010 nm. This spike occurs over a very narrow region and has a negligible impact on the impulse response.

Another notable difference between the two photodetectors is that the response time of the MUTC-4 is governed by both RC and transit-time contributions, while that of the MUTC-9 is predominantly governed by RC effects. If a photodetector is transit-time limited, its impulse response tends to be sharper, and for RC-limited photodetectors, the impulse response is smoother due to the RC low-pass-filtering effect. As a result, the RC-limited photodetector power spectrum has less pronounced spectral features and the phase noise is less impacted by device nonlinearity.

Optics EXPRESS

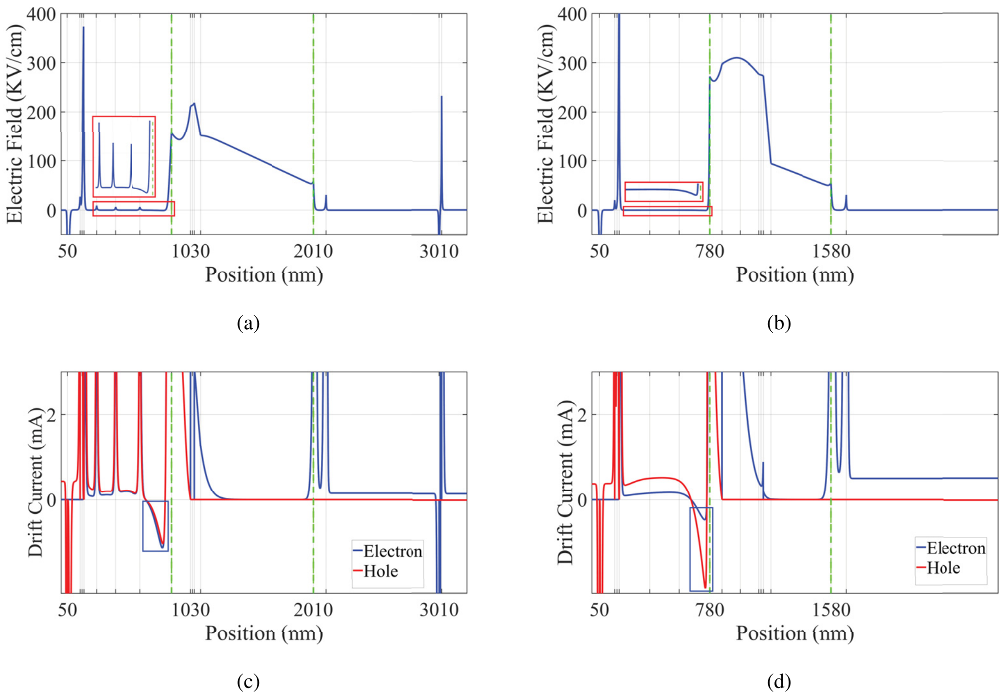

Fig. 3. Electric field in the (a) MUTC-4 and (b) MUTC-9 photodetectors at 1 ps. Negative electric fields appear on the left side of the regions highlighted in the insets with rectangles. The entire field evolution over time may be viewed in Visualization 1 and Visualization 2 for the MUTC-4 and MUTC-9 photodetectors respectively. Electron and hole drift currents in the (c) MUTC-4 and (d) MUTC-9 photodetectors. Regions with negative currents are highlighted with rectangles. The vertical dashed green lines indicate the boundaries of the intrinsic region, and the vertical grid lines indicate the layer boundaries. The entire evolution of the electron drift current may be viewed in Visualization 3 and Visualization 4 respectively.

5. Reduction of phase noise

In order to obtain lower phase noise at higher frequencies, it is necessary to increase the denominator in Eq. (1), which can be done by shortening the tail of the impulse response. A shorter impulse response in the time domain leads to a broader power spectrum, since the denominator in Eqs. (1) and (9) falls off more slowly as the frequency increases. At lower frequencies, a shorter tail reduces the numerator, which can lead to lower phase noise. However, due to the irregular shape of the impulse response, there can be a dip in the power spectrum at any frequency. A dip in the power spectrum would lead to higher phase noise at that frequency since the denominator and the power spectrum are related as can be seen in Figs. 2(b) and (d) as well. As a rule of thumb, a shorter tail on the impulse response will lead to lower phase noise, but the details of the complex carrier transport leads to a complex impulse response and hence a complex power spectral density. Hence, a shorter tail does not always lead to lower phase noise at any particular frequency, although it would lead to lower phase noise over a wide range of frequencies below a critical frequency as discussed in Sec. 3. The critical frequency can be estimated as the frequency below which Eq. (6) is satisfied. For the 2-GHz repetition frequency that we are considering, the critical frequency is approximately 20 GHz. In the previous section we discussed the carrier transport dynamics and design considerations that lead to a shorter impulse response tail and hence a lower phase noise below critical frequency. These findings can be utilized to reduce phase noise below the critical frequency when designing photodetectors.

The steady-state electric field distribution goes through spatial and temporal variations throughout the course of the impulse response due to space-charge effects. The velocity also changes nonlinearly as the electric field varies [1]. The electric field can be engineered in a way such that the electron velocity is maximized spatially and temporally throughout the course of the impulse response. However, it is challenging to find the optimal electric field distribution manually due to the complexity of the nonlinear process that creates the impulse response. The bias voltage and input optical power also play a role in determining phase noise [9]. At each frequency, a given photodetector structure has an optimal bias voltage and input optical power; likewise, for a given bias voltage and input power, there is an optimal photodetector structure. With the availability of computing resources and advancements in optimization algorithms, the optimal photodetector structure or operating conditions can be found using optimization algorithms after formulating an objective function and choosing the relevant device parameters as the optimization parameters. Our approach of calculating phase noise using fast solutions of drift-diffusion equations [9] instead of complex Monte Carlo simulations [3] makes it possible for us to take advantage of recent advancements in optimization algorithms and machine learning techniques [26,27].

6. Optimized MUTC photodetector

We formulated a dual-objective cost function $[2/(1/P + 1/Q) - 1]$, where P and Q are the normalized phase noise and quantum efficiency at 10 GHz, respectively. The cost function was defined so as to minimize phase noise and maximize quantum efficiency. We chose the layer thicknesses and doping densities of the newer MUTC-9 to be the initial parameters in the optimization process. Since the optimization problem that we have is complex, non-convex, and high-dimensional, we used particle swarm optimization [26], which is an evolutionary metaheuristic optimization algorithm. Evolutionary optimization algorithms are a subset of metaheuristic optimization algorithms that have proven to be quite effective in the design of photodetectors [26–28]. We ran the optimization for 24 hours on the UMBC High Performance Computing Facility (HPCF).

In Figs. 4(a) and 4(b), we show the structure and the impulse response of the optimized MUTC-9. In Fig. 5 we show the calculated phase noise of the optimized design. We see that phase noise has improved in the range of 2–200 GHz except for the frequencies from 56–96 GHz. The optimized device has a 3-dB bandwidth that is 43% and 84% higher than the 3-dB bandwidths of the MUTC-4 and MUTC-9 photodetectors, respectively; the RC and transit time bandwidths are closely matched, indicating a well-balanced design that efficiently utilizes both carrier transport dynamics and circuit characteristics. It has a 10% lower and 15% higher quantum efficiency than the MUTC-4 and MUTC-9 photodetectors, respectively. With an optical pulse excitation that is less than 1 ps long, the MUTC-4 remains linear up to approximately 18 mA before exhibiting saturation; the MUTC-9 maintains linearity up to approximately 26 mA, while the optimized MUTC-9 saturates at around 17 mA, indicating a trade-off in saturation current that results from the optimization. The performance metrics of the three photodetectors are listed in Table 1.

Table 1. Performance comparison of the three MUTC photodetector designs

Performance Metric	MUTC-4	MUTC-9	Optimized MUTC
Quantum Efficiency	0.52	0.41	0.47
Bandwidth	17.06 GHz	13.23 GHz	24.45 GHz
Phase Noise at 10 GHz	−173.1 dBc/Hz	−170.53 dBc/Hz	−176.8 dBc/Hz
Saturation Current	18 mA	26 mA	17 mA

Optics EXPRESS

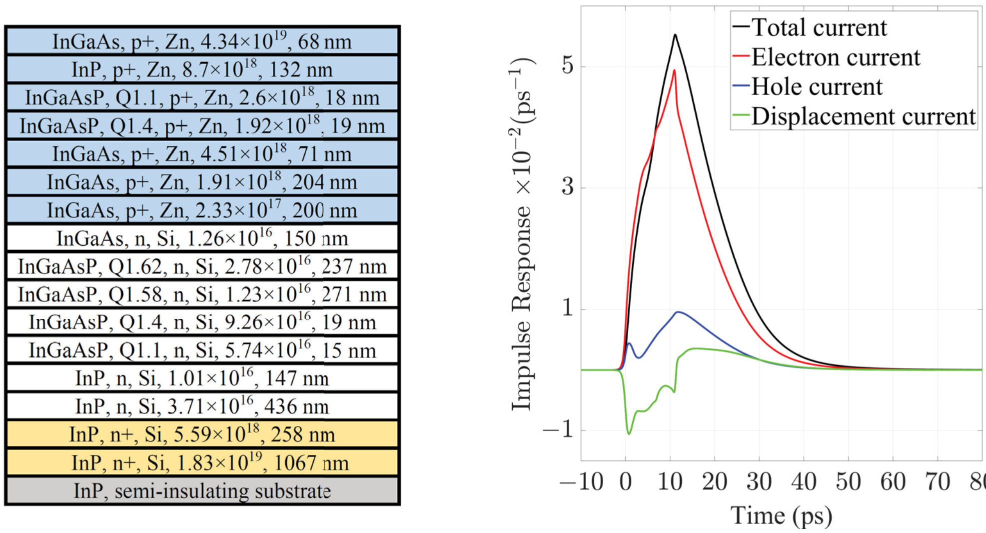

Fig. 4. Structure of (a) the optimized MUTC-9. Blue indicates the *p*-region, yellow indicates the *n*-region, white indicates the *i*-region and grey indicates the substrate. (b) The impulse response of the optimized MUTC-9.

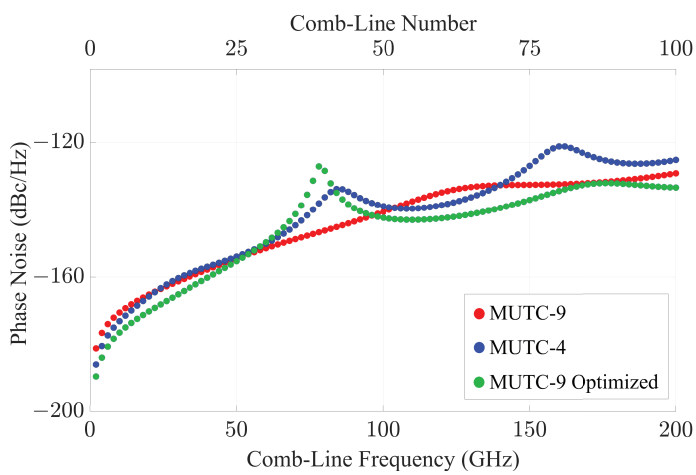

Fig. 5. Optimized MUTC-9 photodetector phase noise vs. comb-line frequency.

Examining the optimized design can reveal the physical mechanisms underlying phase noise improvement as was done in [26]. In Sec. 4, we discussed ways to shorten the impulse response tail and reducing phase noise. We find that the optimization algorithm has successfully implemented the mechanisms that we discussed; it created electric fields at the p-region layer interfaces and also optimized the intrinsic region electric field distribution to take advantage of the nonlinear electron velocity. As a result, the optimized device has a shorter impulse response tail and so a faster response time. We note that in the optimized design the intrinsic region is longer, which should increase transit time, but lengthening the intrinsic region also brings down the overall electric field which leads to better utilization of the nonlinear relationship between electron drift velocity and electric field.

7. Conclusion

We have calculated the phase noise as a function of comb-line frequencies from 2–200 GHz for two MUTC photodetectors. We found that the phase noise increases non-monotonically as a function of comb-line frequency and comb-line number. The non-monotonic increase is due to the complex structure of the current pulse that emerges from the photodetector. We investigated the physics behind the temporal fluctuations in the impulse response, and we found that they are due to a complex interplay of the heterostructure design, the drift velocity as a function of the electric field, and the space charge effect. We conclude that phase noise at comb-line frequencies below 20 GHz can be reduced by shortening the tail of the impulse response. However, this overall reduction does not apply uniformly to all comb-line frequencies, and achieving a reduction at a particular comb-line frequency or range of comb-line frequencies requires a separate optimization. Finally, we presented ways to reduce the phase noise and presented an optimized MUTC photodetector design.

We model carrier transport using a single electron gas (SEG) approximation [29], which assumes that the scattering between different phase-space valleys is effectively instantaneous. This assumption becomes less valid when the device layers become thin and when response times of the order of a picosecond or less are considered. The primary goal of this study is to investigate the sources of nonlinearity in phase noise in these photodetectors and to develop an optimization framework. For this purpose we feel that the SEG approximation provides sufficient accuracy. For higher-accuracy prediction of phase noise, a two-valley drift-diffusion model would be required and is being considered for future work.

Funding. U.S. Naval Research Laboratory (N00173-21-1-G901).

Acknowledgments. A portion of our computational work was carried out at the UMBC High Performance Computing Facility (https://hpcf.umbc.edu). Work at UMBC was supported by the Naval Research Laboratory, grant number N00173-21-1-G901.

Disclosures. The authors declare no conflicts of interest.

Data availability. Data underlying the results presented in this paper are not publicly available at this time but may be obtained from the authors upon reasonable request.

References

1. Y. Hu, B. S. Marks, C. R. Menyuk, *et al.*, "Modeling Sources of Nonlinearity in a Simple p-i-n Photodetector," J. Lightwave Technol. **32**(20), 3710–3720 (2014).
2. K. J. Williams, R. D. Esman, and M. Dagenais, "Nonlinearities in p-i-n microwave photodetectors," J. Lightwave Technol. **14**(1), 84–96 (1996).
3. W. Sun, F. Quinlan, T. M. Fortier, *et al.*, "Broadband noise limit in the photodetection of ultralow jitter optical pulses," Phys. Rev. Lett. **113**(20), 203901 (2014).
4. T. Ishibashi, N. Shimizu, S. Kodama, *et al.*, "Uni-Traveling-Carrier Photodiodes," *Ultrafast Electronics and Optoelectronics*, M. Nuss and J. Bowers, eds., Vol. 13 of OSA Trends in Optics and Photonics Series (Optica Publishing Group, 1997), paper UC3.
5. Z. Li, H. Pan, H. Chen, *et al.*, "High-saturation-current modified uni-traveling-carrier photodiode with cliff layer," IEEE J. Quantum Electron. **46**(5), 626–632 (2010).

Optics EXPRESS

6. F. Quinlan, "The photodetection of ultrashort optical pulse trains for low noise microwave signal generation," Laser Photonics Rev. **17**(12), 2200773 (2023).
7. F. Quinlan, T. M. Fortier, H. Jiang, *et al.*, "Analysis of shot noise in the detection of ultrashort optical pulses," J. Opt. Soc. Am. B **30**(6), 1775–1785 (2013).
8. F. Quinlan, T. M. Fortier, H. Jiang, *et al.*, "Exploiting shot noise correlations in the photodetection of ultrashort optical pulse trains," Nat. Photonics **7**(4), 290–293 (2013).
9. S. E. Jamali Mahabadi, S. Wang, T. F. Carruthers, *et al.*, "Calculation of the impulse response and phase noise of a high-current photodetector using the drift-diffusion equations," Opt. Express **27**(3), 3717–3730 (2019).
10. Bahaa E. A. Saleh and Malvin Carl Teich, *Fundamentals of Photonics* (Wiley, 1991).
11. V. J. Urick, Keith J. Williams, and Jason D. McKinney, *Fundamentals of Microwave Photonics* (Wiley, 2015).
12. I. M. Anjum, S. E. Jamali Mahabadi, E. Simsek, *et al.*, "Calculation of the Phase Noise at Comb-Line Frequencies in a Frequency Comb," in *Frontiers in Optics + Laser Science 2021*, C. Mazzali, T. T. C. Poon, R. Averitt, and R. Kaindleds., Technical Digest Series (Optica Publishing Group, 2021), paper JTh5A.122.
13. J. Zang, X. Xie, Q. Yu, *et al.*, "Reduction of Amplitude-to-Phase Conversion in Charge-Compensated Modified Unitraveling Carrier Photodiodes," J. Lightwave Technol. **36**(22), 5218–5223 (2018).
14. X. Xie, J. Zang, A. Beling, *et al.*, "Characterization of Amplitude Noise to Phase Noise Conversion in Charge-Compensated Modified Unitravelling Carrier Photodiodes," J. Lightwave Technol. **35**(9), 1718–1724 (2017).
15. Y. Hu, C. R. Menyuk, X. Xie, *et al.*, "Computational Study of Amplitude-to-Phase Conversion in a Modified Unitraveling Carrier Photodetector," IEEE Photonics J. **9**(2), 1–11 (2017).
16. J. Taylor, F. Quinlan, and S. Diddams, "Characterization of noise properties in photodetectors: a step toward ultra-low phase noise microwaves," in *41st Annu. Precise Time and Time Interval Syst. Appl. Meeting* (2009), pp. 339–348.
17. D. von der Linde, "Characterization of the noise in continuously operating mode-locked lasers," Appl. Phys. B **39**(4), 201–217 (1986).
18. I. M. Anjum, E. Simsek, S. E. Jamali Mahabadi, *et al.*, "Sources of Nonlinearity in Phase Noise of MUTC Photodetectors at Comb-Line Frequencies," in *IEEE Photonics Conference (IPC)* (IEEE, 2024), pp.1–2.
19. Y. Hu, T. F. Carruthers, C. R. Menyuk, *et al.*, "Modeling nonlinearity in a modified uni-traveling-carrier (MUTC) photodetector," in *IEEE Photonics Conference (IPC)* (IEEE, 2015), pp.122–123.
20. E. Simsek, I. Md Anjum, T. F. Carruthers, *et al.*, "Fast Evaluation of RF Power Spectrum of Photodetectors with Windowing Functions," IEEE Trans. Electron Devices **70**(7), 3643–3648 (2023).
21. E. Simsek, I. M. Anjum, T. F. Carruthers, *et al.*, "Non-Uniform Time-Stepping For Fast Simulation of Photodetectors Under High-Peak-Power, Ultra-Short Optical Pulses," in *International Conference on Numerical Simulation of Optoelectronic Devices (NUSOD)* (2022), pp.1–2.
22. T. P. Pearsall, "Impact ionization rates for electrons and holes in $Ga_{0.47}In_{0.53}As$," Appl. Phys. Lett. **36**(3), 218–220 (1980).
23. K. Yang, J. R. East, and G. I. Haddad, "Numerical modeling of abrupt heterojunctions using a thermionic-field emission boundary condition," Solid-State Electron. **36**(3), 321–330 (1993).
24. J. Callaway, "Optical absorption in an electric field," Phys. Rev. **130**(2), 549–553 (1963).
25. B. O. Seraphin and N. Bottka, "Franz–Keldysh effect of the refractive index in semiconductors," Phys. Rev. **139**(2A), A560–A565 (1965).
26. I. M. Anjum, E. Simsek, S. E. Jamali Mahabadi, *et al.*, "Use of Evolutionary Optimization Algorithms for the Design and Analysis of Low Bias, Low Phase Noise Photodetectors," J. Lightwave Technol. **41**(23), 7285–7291 (2023).
27. I. M. Anjum, E. Simsek, S. E. Jamali Mahabadi, *et al.*, "Design and Analysis of Low Bias, Low Phase Noise Photodetectors for Frequency Comb Applications Using Particle Swarm Optimization," in *IEEE International Topical Meeting on Microwave Photonics (MWP)* (2022), pp.1–4.
28. I. M. Anjum, E. Simsek, S. E. Jamali Mahabadi, *et al.*, "Dual-Objective Numerical Optimization of MUTC Photodetectors for Frequency Comb Applications," in *IEEE Research and Applications of Photonics in Defense Conference (RAPID)* (2023), pp.1–2.
29. K. Blotekjaer, "Transport equations for electrons in two-valley semiconductors," IEEE Trans. Electron Devices **17**(1), 38–47 (1970).